NeuroImage 206 (2020) 116333

Contents lists available at ScienceDirect

NeuroImage

journal homepage: www.elsevier.com/locate/neuroimage

Predicting individual decision-making responses based on single-trial EEG

Yajing Si [a,b,1], Fali Li [a,b,1], Keyi Duan [a,b], Qin Tao [a,b], Cunbo Li [a,b], Zehong Cao [c,d], Yangsong Zhang [a,b,e], Bharat Biswal [a,b,f], Peiyang Li [g], Dezhong Yao [a,b], Peng Xu [a,b,*]

[a] The Clinical Hospital of Chengdu Brain Science Institute, MOE Key Lab for Neuroinformation, University of Electronic Science and Technology of China, Chengdu, 611731, China
[b] School of Life Science and Technology, Center for Information in Medicine, University of Electronic Science and Technology of China, Chengdu, 611731, China
[c] Centre for Artificial Intelligence and Faculty of Engineering and Information Technology, University of Technology Sydney, NSW, Australia
[d] Discipline of ICT, School of Technology, Environments and Design, University of Tasmania, Hobart, Australia
[e] School of Computer Science and Technology, Southwest University of Science and Technology, Mianyang, 621010, China
[f] Department of Biomedical Engineering, New Jersey Institute of Technology, Newark, NJ, 07102, USA
[g] School of Bioinformatics, Chongqing University of Posts and Telecommunications, Chongqing, China

ARTICLE INFO

Keywords:
Decision-making
Electroencephalogram (EEG)
Discriminative spatial network pattern
Brain network
Single-trial prediction

ABSTRACT

Decision-making plays an essential role in the interpersonal interactions and cognitive processing of individuals. There has been increasing interest in being able to predict an individual's decision-making response (i.e., acceptance or rejection). We proposed an electroencephalogram (EEG)-based computational intelligence framework to predict individual responses. Specifically, the discriminative spatial network pattern (DSNP), a supervised learning approach, was applied to single-trial EEG data to extract the DSNP feature from the single-trial brain network. A linear discriminate analysis (LDA) trained on the DSNP features was then used to predict the individual response trial-by-trial. To verify the performance of the proposed DSNP, we recruited two independent subject groups, and recorded the EEGs using two types of EEG systems. The performances of the trial-by-trial predictors achieved an accuracy of 0.88 ± 0.09 for the first dataset, and 0.90 ± 0.10 for the second dataset. These trial-by-trial prediction performances suggested that individual responses could be predicted trial-by-trial by using the specific pattern of single-trial EEG networks, and our proposed method has the potential to establish the biologically inspired artificial intelligence decision system.

1. Introduction

Decision-making is a complex cognitive process triggered by daily choices and is always associated with emotion, personality, and motivation (Cecchetto et al., 2017; Hastie, 2001; Preuss et al., 2016; Sanfey, 2007). Decision-making plays an essential role in interpersonal interactions and social stabilities across cultures (Basten et al., 2010; Si et al., 2018). The reliable prediction of individual responses to different fairness conditions (i.e., how the subject makes decisions with preference) is helpful in the establishment of a natural and responsive artificial intelligence system (Long et al., 2012a). Recent studies have tried to predict the individual decision responses from different aspects. For example, the best-fitting computational model utilized both expected and experienced feelings about potential outcomes to predict choices, which revealed that the loss aversion in decision-making was explained by an asymmetry in how feelings about losses and gains were weighted when making a choice (Charpentier et al., 2016). The effect of approximate numeric abilities could also be considered a factor that can predict objectively advantageous decision-making, even beyond the effects of executive functions (Mueller et al., 2018). In terms of intrinsic resting-state brain activity, the functional connectivity among the brain regions derived from functional magnetic resonance imaging (fMRI) was utilized to predict individual impulsivity of decision-making, suggesting that the functional connectivity of the human brain may be a biomarker of decision impulsivity (Li et al., 2013).

However, the existing approaches predicting individual decision response mainly focused on the averaged measurements of the neurophysiological data, and the averaging across multiple identical trials

* Corresponding author. The Clinical Hospital of Chengdu Brain Science Institute, MOE Key Lab for Neuroinformation, University of Electronic Science and Technology of China, No. 2006, Xiyuan Ave, West Hi-Tech Zone, Chengdu, Sichuan, 611731, China.
E-mail address: xupeng@uestc.edu.cn (P. Xu).
[1] Y. Si and F. Li contribute equally to this paper.

https://doi.org/10.1016/j.neuroimage.2019.116333
Received 19 July 2019; Received in revised form 2 October 2019; Accepted 2 November 2019
Available online 4 November 2019

typically discards information about trial-to-trial variability (Blankertz et al., 2011), while this variability can be a consequence of variation in the design and can also reflect the varied individual states (Ratcliff et al., 2009). Although a large amounts of efforts has been invested, the accurate prediction of decision response for an individual remains far from accurate, especially online, where it is urgently required by the practical human-computer interaction (HCI) systems. In essence, the reliable prediction is largely dependent on how the neural mechanism underlying decision-making is revealed. Decision-making engages multiple brain areas, such as the frontal lobe, insula, parietal lobe, and anterior cingulate cortex (ACC) (Bartra et al., 2013; Buschman and Miller, 2007; Critchley et al., 2000; Krain et al., 2006; Suzuki et al., 2012). The interactions among these brain regions have also been demonstrated to contribute to the decision-making. When making a decision, the association between the right insula and the inferior frontal cortex plays a crucial role in the integration of bottom-up, sensory information with top-down, response-related information to goal-directed behavior (Dodds et al., 2010). The reward-guided decision also depends on a brain network that involves the frontal lobe and ACC, and even macaque monkeys recruited similar regions during reward-guided decision-making tasks (Neubert et al., 2015). Moreover, one current study utilizing the time-varying network analysis of scalp EEG also reveals that, when subjects perform the different decision responses, the distinct network patterns can be observed (Si et al., 2018).

Neurophysiological signals, such as electroencephalogram (EEG) and (fMRI), are known to contain the important decision information that can be utilized for decision assessment (Bénar et al., 2007; Blankertz et al., 2011). In addition to accuracy, another aspect that is important for the prediction system is the timely requirement, i.e., the online prediction. Therefore, EEG, with its high temporal resolution and easy setup, provides the potential to establish a practical decision-making prediction system. To realize the online prediction, it is necessary to establish a trial-by-trial analysis approach to predict the individual response using single-trial EEG.

However, though some existing studies have probed the prediction of decision making behavior, those previous works mainly paid more attention to predict the overall individual behavioral response (LvC et al., 2019; NK Glober and TM Abramson, 2019), i.e., the acceptance rates after the whole DM experiment instead of the instantaneous response of subject during experiment. For example, neurocognitive indicators of disinhibition (stop signal reaction time) and decision-making (card playing task) could effectively predict relapse in pathological gamblers to guide the corresponding treatment plan (Goudriaan et al., 2008). Recently, regional homogeneity patterns in the dorsal prefrontal cortex were examined to predict individual differences in decision impulsivity (LvC et al., 2019). These indexes across multiple identical trials will inevitably lose information reflected by trial-to-trial variability, and the single-trial based prediction that can provide the instantaneous information for subject's DM behavior has not been reported yet. There has been growing interest to the single-trial detection of human cognition functions, which has the potential to establish the biologically inspired artificial intelligence systems (Hsu, 2013; Hsu et al., 2007; S Debener et al., 2006). In this study, motivated by the involved networks in decision-making, we aimed to develop an EEG-based computational intelligence framework to predict the individual trial-by-trial response in decision-making. To fulfill this aim, the EEG data sets were collected when subjects participated in an Ultimatum Game (UG) task. Thereafter, based on the single-trial networks of distinct decision responses (i.e., acceptance and rejection), we analyzed the topological differences between acceptance and rejection to examine the neural mechanism underlying decision-making. Considering the rather lower signal to noise ratio (SNR) of a single EEG trial, the supervised learning was then adapted to extract the discriminative spatial network topology in single-trial EEG. A linear discriminate analysis (LDA) classifier that was trained by the discriminative spatial network topology was adopted to perform the single-trial prediction of individual responses in the UG task. Finally, to investigate the reliability of our proposed approach, these analyses were replicated on two independent EEG data sets recorded by two different EEG systems from two independent subject groups.

2. Material and methods

2.1. Participants

Two independent groups (datasets A and B) of subjects participated in this study at the University of Electronic Science and Technology of China (UESTC). None of the subjects had a history of neurological or psychiatric disorders, and they were not currently using any psychoactive medications. The experiment protocol was approved by the Institution Research Ethics Board of the UESTC. Informed consent was obtained from all subjects before they joined the study.

2.2. Experimental protocol

In this study, we adopted the UG to simulated actual decision-making, which is a typical dyadic bargaining situation that can be utilized to explore physiological correlates of the decision processing (Koenigs and Tranel, 2007). Various studies have proved that UG can simulate the actual decision-making well, and it can reflect fairness consideration in asset division and highlight the social context that influences social decisions and outcome processing, partially depending on inter-individual differences (Horat et al., 2017; Peterburs et al., 2017; Wu et al., 2011). The experiments were performed in a quiet, dimly light room. In the first 2 min, subjects were instructed to take deep breaths to adapt to the experimental environment. Then, 5 min of eye-closed resting-state EEG data sets were recorded prior to the UG task. Thereafter, subjects participated in the UG task that lasted approximately 8.5 min.

In the UG task, the subject (responder) was prompted to decide whether to accept an offer of the proposer (the computer). If the subject accepted the offer, both players (the responder and the proposer) received the money provided by the proposer; on the contrary, they would earn nothing. During the experiment, the subjects were instructed to be the role of the responder in every trial, and then they were told to play the game with another subject, i.e., the proposer, who sat in another room.

Fig. 1 shows the timeline of the UG. In the experiment, the sum was splits of ¥ 10. The experiment included three categories of conditions: the fair offers (¥ 5: ¥ 5) and the unfair offers, which consisted of extremely (¥ 1: ¥ 9) and moderately unfair (¥ 3: ¥ 7) offers. Subjects received 90 offers that were randomly chosen by the computer, with 30 trials for each of the three conditions. Each trial lasted a period of 800 ms starting with the presentation of a fixation crosshair. Then, a note lasting with 500 ms was given to indicate the amount of the sum. After 1000 ms of black screen, the proposed offer was presented for 1500 ms. During this interval, the subjects were required to decide to reject (press the button "3" key on the keyboard) or accept (press the button "1" key on the keyboard) the offer. Subsequently, the players would receive the amount of money assigned to them on that trial, and the cumulative amount of the subject's winnings were simultaneously presented for 1200 ms after pressing the response key. Before a formal session, all subjects were required to try a preliminary round to ensure that the rules of the game were clear.

2.3. EEG data acquisition

For Group A, the BrainAmp amplifier (Brain Products GmbH), hereinafter termed amplifier-1, was used to collect the EEG data sets. Electrodes FCz and AFz served as the reference and ground, respectively. For Group B, the ASA-Lab amplifier (ANT Neuro), termed amplifier-2, was adopted, along with the reference and ground being assigned as electrodes CPz and AFz, respectively. The 64-channel UG-EEG data sets of both groups were recorded and digitized with a sampling rate of 500 Hz. The electro-oculogram (EOG) was recorded from an extra electrode

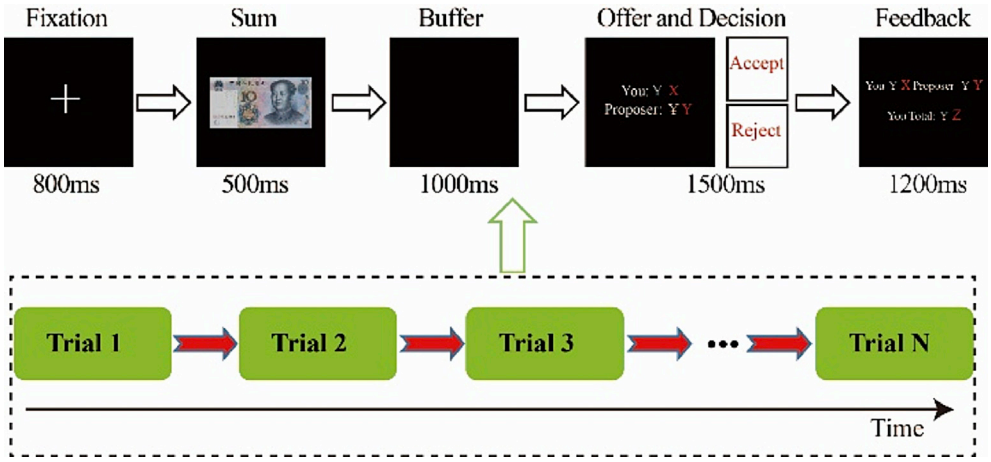

Fig. 1. Timeline of the UG. In each trial, subjects decided to accept or reject the proposed offer.

located above the side of the left eye to monitor eye movements. Throughout the entire experiment, the impedance of each electrode was maintained below 5 kΩ.

2.4. A single-trial EEG-based prediction framework

In this study based on two independent EEG data sets, we proposed an EEG-based single-trial prediction framework to predict individual decision response, including EEG preprocessing, EPRs extraction, brain network construction, network properties calculation, and single-trial prediction based on the discriminative spatial network pattern (DSNP). The first group (dataset A) consisted of 14 subjects (8 males and 6 females, age range: 21–26 years, and mean age: 23.29 years), and the BrainAmp amplifier manufactured by Brain Products GmbH was used for EEG recording. In the second group (dataset B), there were 20 subjects (16 males, and 4 females, age range: 19–25 years, mean age: 22.27 years), and the ASA-Lab amplifier provided by ANT Neuro was adopted for EEG recording.

2.4.1. Data preprocessing

The preprocessing pipeline was targeted to acquire reliable acceptance and rejection trials for each subject. The preprocessing procedures included the common average reference, 1–20 Hz band-pass filtering (Si et al., 2018), [-200 ms, 800 ms] data segmenting, [-200 ms, 0 ms] baseline correcting, artifact trial removal (±60 μV as threshold), and single-trial denoising on each electrode by using the wavelet toolkit (Cai and Silverman, 2001).

2.4.2. EPRs extraction

The medial frontal negativity (MFN, 220 ms–350 ms, 0 ms: the onset of stimulus) is an important EEG component during the processing of decision-making (Peterburs et al., 2017). Therefore, we first evaluated whether the decision-making related MFN component could predict the responses of decision-making based on a single EEG trial. MFN amplitude was subsequently extracted from the single trial ERP on F3, Fz and F4, where the MFN usually occurs (Wang et al., 2016). Considering the latency effect on MFN estimation, the MFN amplitude is defined as the mean amplitude in the time window ±20 ms, with the largest negative MFN peak at the center (Fig. 2). After MFN was extracted from the three electrodes, the three MFN amplitudes were combined together to form a 3 dimensional feature for the prediction of decision-making response based on each single trial EEG.

2.4.3. Network construction

Coherence (COH) is one of the most commonly used methods to analyze the synchrony-defined cortical neuronal assemblies, which could

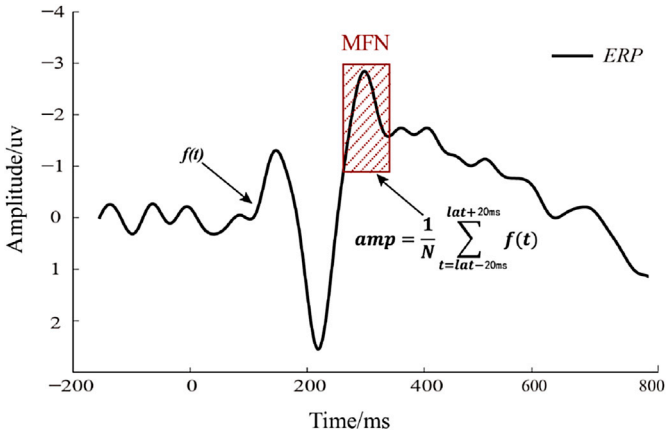

Fig. 2. The definition of MFN amplitude. It was the mean value of 20 sample points in the 40-ms time window centered at the peak.

capture the coupling in the frequency domain (Thatcher et al., 2005; Xu et al., 2014). Previous studies have revealed that the relationship between brain network and cognition functions, such as attention and motor imagery, could be analyzed efficiently by the COH method (Li et al., 2018; Zhang et al., 2015). COH measures the linear relationship at a specific frequency between two signals $X(t)$ and $Y(t)$ based on their cross- and auto-spectrum. In this study, we thereby adopted frequency-specific COH to estimate the connection strength between pairs of network nodes. Mathematically, COH is expressed as follows:

$$C_{XY}(f) = \frac{|P_{XY}(f)|^2}{P_{XX}(f)P_{YY}(f)} \quad (1)$$

where $P_{XY}(f)$ is the cross-spectrum of $X(t)$ and $Y(t)$ at frequency f, and $P_{XX}(f)$ and $P_{YY}(f)$ indicate the auto spectrum at frequency f estimated from the Welch-based spectrum of $X(t)$ and $Y(t)$, respectively.

The coherence is computed from the entire single trial (i.e., the 1 s from −200 ms to 800 ms), and the frequency band employed is from 1 to 20 Hz. The connection strength between each pair of nodes was acquired by averaging the COH values within the concerned frequency band. The 21 canonical electrodes (FP1, FPz, FP2, F7, F3, Fz, F4, F8, T7, C3, Cz, C4, T8, P7, P3, Pz, P4, P8, O1, O2, Oz) of the 10–20 system were used to construct the brain network to reduce the effect of volume conduction (Li et al., 2016). In amplifier-1 in the current study, however, only 12 electrodes (F3, Fz, F4, C5, Cz, C6, P3, Pz, P4, O1, Oz, O2) of the 21 canonical electrodes consistently worked well across all the subjects, and they were therefore selected and used to construct the brain network. For

amplifier-2, 21 canonical electrodes consistently worked well during the UG experiment across subjects and were used in further analysis. After calculating the COH between each pair of electrodes, the 12×12 or 21×21 weighted adjacency (connectivity) matrix was achieved to denote interactions among the 12 or 21 nodes for each trial. Then, the brain network was constructed based on the 12×12 (or 21×21 for amplifier-2) weighted adjacency (connectivity) matrix using the corresponding COH as the network edge between nodes i and j, where C_{ij} is the edge linkage strength between nodes i and j obtained by Eq. (1).

2.4.4. Network properties

To quantitatively measure the single-trial brain network, four network properties, namely clustering coefficient (Clu), global efficiency (*Ge*), local efficiency (*Le*), and characteristic path length (*L*) were then calculated (Li et al., 2018, 2019b). The detailed definitions of these properties were formulated as follows,

$$Clu = \frac{1}{NW}\sum_{i\in\theta}\frac{\sum_{j,l\in\theta}\left(C_{ij}C_{il}C_{jj}\right)^{1/3}}{\sum_{j\in w_{ij}}\left(\sum_{j\in\theta}C_{ij}-1\right)} \tag{2}$$

$$L_e = \frac{1}{NW}\sum_{i\in\theta}\frac{\sum_{j,l\in\theta j\neq i}\left(C_{ij}C_{il}\left[d_{jl}(\theta_i)\right]^{-1}\right)^{1/3}}{\sum_{j\in\theta}C_{ij}\left(\sum_{j\in\theta}C_{ij}-1\right)} \tag{3}$$

$$G_e = \frac{1}{NW}\sum_{i\in\theta}\frac{\sum_{j\in\theta,j\neq i}d_{ij}^{-1}}{NW-1} \tag{4}$$

$$L = \frac{1}{NW}\sum_{i\in\theta}L_i = \frac{1}{NW}\sum_{i\in\theta}\frac{\sum_{j\in\theta,j\neq i}d_{ij}}{NW-1} \tag{5}$$

where d_{ij} is the shortest weighted path length between i and j, NW is the node number, and θ is the set of all nodes in a single-trial network. Specifically, *Clu* is defined as the fraction of triangles around an individual network node. L_e is the average efficiency of the local subgraphs. *Clu* and L_e are related to the estimation of the potential for functional segregation between brain regions. *Ge* is the average efficiency of the related brain network, and *L* is the mean value of the shortest path length between all pairs of network nodes.

2.4.5. DSNP-based single-trial prediction

While the network topology determines the network properties, the network properties alone cannot fully describe the network topology. Given that different cognitive tasks give rise to different network structures (Dixon et al., 2017; Li et al., 2016; Young et al., 2017), it is plausible that formal mathematical discrimination of spatial topology could differentiate different tasks. Therefore, we tested the discriminative spatial network pattern, a supervised learning approach, as a tool for single-trial prediction. An overview of the procedure is depicted in Fig. 3.

As illustrated in Fig. 3, to simulate an online condition, we supposed N trials in the UG task for one subject, then divided the N trials into training and testing sets based on the presented time, where the former $N/2$ trials occurring relatively earlier served as the training set, and the remaining $N/2$ trials were used as the testing set. Therefore, the DSPN-based single-trial prediction consisted of the training and single-trial prediction procedures. The training procedure has two aims in this prediction framework, one is to train the predictor model, and another is to learn the spatial filters that can be used to extract DSNP feature for the testing trials. To fulfill this goal, in the training procedure as shown in Fig. 3(a), after we calculated the coherence network of each trial (Zhang et al., 2015), we use the DSNP to estimate the spatial filter and then to extract the discriminative spatial pattern of the weighted brain network based on the training set (Xu et al., 2014). Finally, the prediction model of DSNP features for different decision responses was trained by the LDA algorithm (Boulgouris and Chi, 2007).

Specifically, we let $C_1(k)$ and $C_2(m)$ be the adjacency matrix for the *k-th* trial of rejection and for the *m-th* trial of acceptance in the training set, respectively. Supposing that there are N_1 trials for rejection and N_2 trials for acceptance with $N_1 + N_2 = N/2$, the mean adjacency matrices for the two responses are defined as,

$$C_1 = \frac{1}{N_1}\sum_{k=1}^{N_1}C_1(k),\ C_2 = \frac{1}{N_2}\sum_{m=1}^{N_2}C_2(m) \tag{6}$$

where C_1 and C_2 are with dimension of 12×12 for amplifier-1 and 21×21 for amplifier-2. Accordingly, C_1 and C_2 contain the spatial network patterns of the acceptance and rejection responses, respectively. To extract the discriminative spatial network pattern, we applied a linear spatial filter p with dimension of 1×12 for the amplifier-1 or 1×21 for the amplifier-2 to the C_1 and C_2 as,

$$Y_1 = pC_1,\ Y_2 = pC_2 \tag{7}$$

The aim of the spatial filter is to enhance the differences of spatial network topology between the two responses, which is equivalent to maximize the following generalized Rayleigh quotient,

$$\arg_p \max J(p) = \frac{Y_1 Y_1^T}{Y_2 Y_2^T} = \frac{pC_1C_1^Tp^T}{pC_2C_2^Tp^T} = \frac{p\Phi_1 p^T}{p\Phi_2 p^T} \tag{8}$$

where Φ_1 and Φ_2 are the covariance matrices of C_1 and C_2, respectively. Considering that the scaling of the projection p will have no effect on the object value, (8) can be transformed into a constrained optimization problem as,

$$\begin{cases}\arg_p \max(p\Phi_1 p^T)\\ s.t. p\Phi_2 p^T = 1\end{cases} \tag{9}$$

Through introducing the Lagrange multiplier, the objective function can be rewritten as,

$$L(p;\lambda) = p\Phi_1 p^T - \lambda(p\Phi_2 p^T - 1) \tag{10}$$

By taking the derivative of (10) with respect to p under the condition $\frac{\partial L}{\partial p} = 0$, the objective projection p can be estimated using the generalized eigenvalue equation as,

$$\Phi_1 p^T = \lambda\Phi_2 p^T \tag{11}$$

where λ denotes the eigenvalue of the generalized eigenvalue equation, and p is the corresponding eigenvector (Benjamin Blankertz et al., 2007). As for the multiple m spatial filters, (11) can be solved as,

$$\Phi_2^{-1}\Phi_1 P^T = \sum P^T \tag{12}$$

where P is a matrix consisting of the eigenvectors of $\Phi_2^{-1}\Phi_1$ and $\sum = diag(\lambda_1, \lambda_2, ..., \lambda_m)$ with λ being the corresponding singular values. In essence, the mapping is a supervised learning approach to enhance the discriminative spatial network pattern between different conditions. For example, when the most discriminative 3 pairs of DSNP spatial filters are utilized, 6-dimensional DSNP features will be obtained (Benjamin Blankertz et al., 2007; Peng Xu et al., 2011). Specifically, the 3 pairs of DSNP filters comprise a matrix $P_{DSPN} = [p_1, p_2, ..., p_6]$ with each filter being a 12-length or 21-length vector, i.e., P_{DSNP} with a dimension of 12×6 or 21×6. The differentiation abilities of the filters were denoted by the eigenvalues in Σ, and the first and last filters corresponding to the largest and smallest eigenvalues consist of the most discriminative DSNP filter pair (Benjamin Blankertz et al., 2008). For a 12×12 or 21×21 adjacency matrix C, the corresponding DSNP feature transformation is

$$F_{DSNP} = \log\left(\mathrm{var}\left(P_{DSNP}^T C\right)\right) \tag{13}$$

which results in a vector of length 6 with var (.) denoting the variance

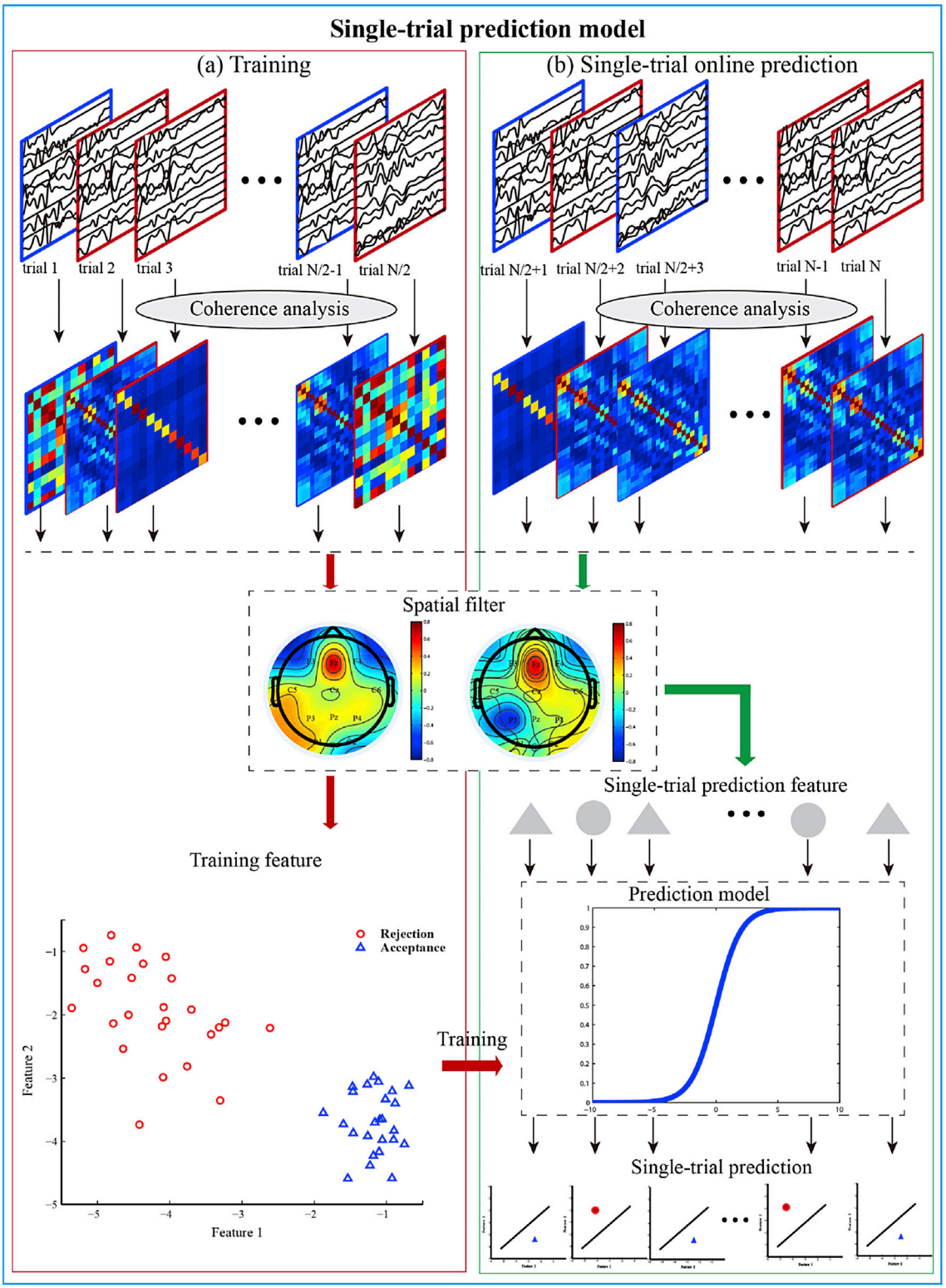

Fig. 3. The detailed procedure of DSNP-based single-trial prediction for different responses (i.e. acceptance and rejection) during decision-making.

operator for the rows of matrix.

Therefore, after training, the corresponding spatial filters and the training features can be estimated from the training set. Then based on the DSNP features extracted in the training set, the LDA predictor is trained for each subject as shown in Fig. 3. Practically, letting $X = \{x_1^a, x_2^a, \ldots, x_m^a, x_1^r, x_2^r, \ldots, x_n^r\}$ be the DSNP features from acceptance and rejection responses, the aim of LDA is to find a vector ω which maximizes (Mika et al., 2002; Ye J and Li, 2005)

$$J(\omega) = \frac{\omega^T S_B \omega}{\omega^T S_W \omega} \tag{14}$$

where

Table 1
Prediction performance for the two datasets through the ERP amplitudes (EA), network properties (NP) and DSNP features.

			ACC	Accept			Reject		
				Precision	Recall	F-measure	Precision	Recall	F-measure
LDA	Amplifier-1 (n = 14)	DSNP	**0.88 ± 0.09**	**0.87 ± 0.10**	**0.95 ± 0.07**	**0.91 ± 0.08**	**0.94 ± 0.08**	**0.85 ± 0.14**	**0.89 ± 0.11**
		EA	0.46 ± 0.05	0.58 ± 0.04	0.44 ± 0.11	0.49 ± 0.08	0.36 ± 0.04	0.50 ± 0.08	0.42 ± 0.04
		NP	0.62 ± 0.12	0.58 ± 0.16	0.55 ± 0.23	0.56 ± 0.18	0.60 ± 0.16	0.63 ± 0.12	0.61 ± 0.12
	Amplifier-2 (n = 20)	DSNP	**0.90 ± 0.10**	**0.87 ± 0.12**	**0.93 ± 0.09**	**0.90 ± 0.09**	**0.93 ± 0.09**	**0.85 ± 0.16**	**0.88 ± 0.12**
		EA	0.48 ± 0.03	0.48 ± 0.03	0.47 ± 0.10	0.47 ± 0.07	0.48 ± 0.03	0.49 ± 0.08	0.48 ± 0.04
		NP	0.65 ± 0.17	0.65 ± 0.17	0.67 ± 0.18	0.65 ± 0.16	0.64 ± 0.19	0.62 ± 0.24	0.62 ± 0.21

ACC is the prediction accuracy.

$$S_B = \sum_{i=1}^{C} n_i(\mu_i - \mu_i)(\mu_i - \mu_i)^T \tag{15}$$

$$S_W = \sum_{i=1}^{C} \sum_{x_k \in class\ I} (\mu_i - x_k)(\mu_i - x_k)^T \tag{16}$$

are the between and within class scatter matrices, respectively. Here, μ_i represents the expectation of the i-th class, C represents the number of the class, and n_i is the samples number of the i-th class and x_k the sample of class i. The theory behind maximizing $J(\omega)$ is to find a direction which maximizes the projected class means (the numerator) while minimizing the class variance in this direction (the denominator).

Based on the DSNP filters and LDA predictor learned from the training set, an online prediction can be performed in Fig. 3(b). Specifically, for the k-th EEG trial that waits for the DSNP-based prediction, three steps need to be taken: calculating the adjacency matrix following (1), using the DSNP filters to extract the DSNP features by (13), and inputting the DSNP features into the trained LDA predictor to get the prediction result of the current trial (Li et al., 2019a).

In this study, following the DSNP-based single-trial prediction procedures depicted above, the corresponding response for each trial could be predicated for each subject. Thereafter, the indices including accuracy (ACC), precision, recall, and F-measure (Cao et al., 2018) were calculated for the two EEG data sets to quantitatively evaluate the prediction performance. When the network properties were used for single-trial prediction, the difference from DSNP is that the four network properties were directly calculated from the adjacency matrix for each trial, which was then used to train the LDA predictor using the network properties extracted from the training set, and also served for the prediction for the trials in the testing set. Similar to the prediction based on network properties, the ERP amplitude based prediction utilizes the MFN features extracted from the training set to train the LDA predictor.

2.4.6. Statistical analysis

In the current study, paired t-tests were utilized to quantify the differences in network topology and network properties between the acceptance and rejection responses. To reveal the statistical prediction performances of different methods (i.e., ERP, network properties and DSNP based approaches), analysis of variance (ANOVA) was used to compare these three methods.

3. Results

The performance of our proposed online single-trial prediction relied heavily on the ability of the DSNP filters to reliably extract the discriminative spatial network patterns between different conditions. Fig. 4(b) shows the differential network patterns between the rejection and acceptance responses in the training set for one subject, where the red and blue lines denote the edges with the significantly stronger and weaker strengths, respectively ($p < 0.05$) for acceptance compared to rejection. However, Fig. 4(c) does not show the significant differences in the corresponding network properties. By contrast, Fig. 4(a) illustrates the pair with the most discriminative DSNP filters, where the nodes shown to have the dense linkages in Fig. 4(b) are emphasized with large values (i.e., marked with either the deep red or deep blue). Fig. 5 then shows the scatter plots of the DSNP features extracted by a pair of the most discriminative DSNP filters in Fig. 4(a) for this subject.

Following the procedure in Fig. 3, we used ERP amplitudes, the four network properties and DSNP features to perform the single-trial prediction of decision response for each subject. As shown in Table 1, when ERP amplitudes were utilized, the prediction accuracies only achieved

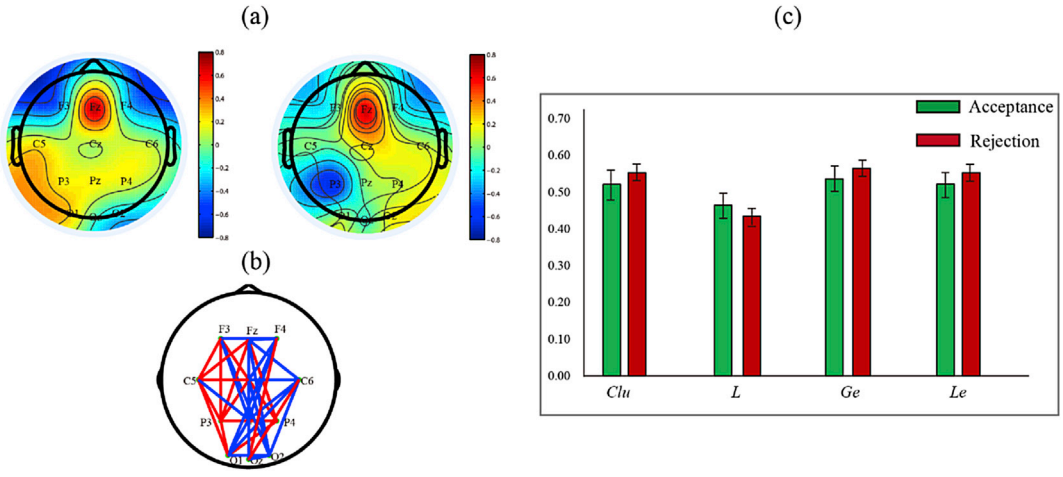

Fig. 4. The scalp topographies for the two most discriminative DSNP filters (Filter 1 and 2), and the network topology differences and the network properties between acceptance and rejection for one subject of the amplifier-1. (a) The scalp topographies of the DSNP filters, (b) the network topology differences, and (c) the network properties. The red lines in (b) denote the network edges with the significantly stronger linkage strengths ($p < 0.05$) of acceptance than rejection, while the blue lines indicate the ones with the significantly weaker linkage strengths.

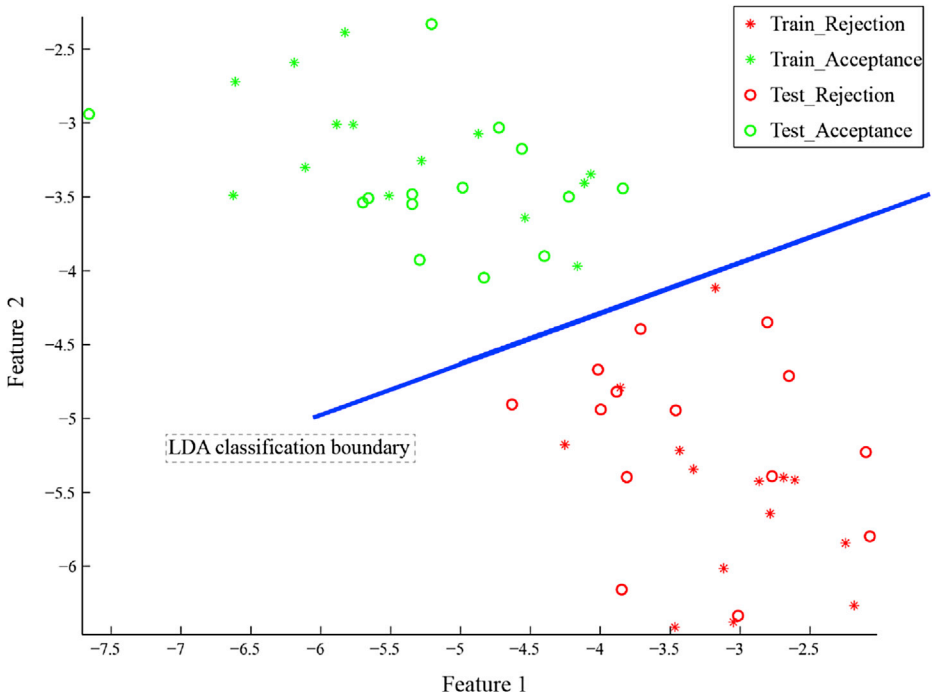

Fig. 5. The scatter plots of the two DSNP features between rejection and acceptance extracted with the two most discriminative DSNP filters.

0.46 ± 0.05 and 0.48 ± 0.03 for two datasets. When network properties were used, the prediction accuracies achieved 0.62 ± 0.12 and 0.65 ± 0.17 for two datasets. Moreover, for the acceptance condition in both datasets, the LDA-based predictor achieved (0.58 ± 0.16 and 0.65 ± 0.17) precision, (0.55 ± 0.23 and 0.67 ± 0.18) recall, and (0.56 ± 0.18 and 0.65 ± 0.16) F-measure. Compared to the performance of ERP amplitudes and network properties, the DSNP consistently achieved significantly ($p < 0.01$) higher accuracies of 0.88 ± 0.09 and 0.90 ± 0.10 for the two datasets, respectively. Concretely, for the acceptance condition, the LDA-based predictor with DSPN feature achieved precision of 0.87 ± 0.10 and 0.87 ± 0.12, recall of 0.95 ± 0.07 and 0.93 ± 0.09, and F-measure of 0.91 ± 0.08 and 0.90 ± 0.09 for the two datasets. The performed ANOVA test revealed that DSNP based approaches showed statistical performance improvement compared to both the ERP and network properties based approaches ($p < 0.01$). Specifically investigating the performances among the three fair conditions, Table 2 consistently shows that the LDA-based predictor could achieve an accuracy above 0.84 accuracy across the three conditions for the two datasets. To further investigate the variability of single-trial prediction performance across subjects, we then plotted the prediction accuracies of subjects achieved by DSNP for each dataset in Fig. 6, which indeed showed the huge variability across subjects (i.e., 0.74–1.00 for amplifier-1 and 0.66–1.00 for amplifier-2). We also found that most of the subjects had prediction accuracies over 0.80 (11/14 for amplifier-1, 17/20 for amplifier-2).

4. Discussion

This study established a framework for the online single-trial prediction of an individual decision response using single-trial EEG. Given that the brain involves different networks to process the related information when subjects perform the varied decision responses, we specifically constructed the single-trial EEG network, and developed an effective approach (i.e., DSNP) to extract the discriminative spatial network pattern for the decision prediction.

As shown in Fig. 4(b), the comparison of brain networks demonstrates the existence of the large network topology difference between the acceptance and rejection. The long-range frontal-parietal/occipital linkages in Fig. 4 (b) indicated that the two regions are important for the decision-making, which has been validated by various fMRI or transcranial magnetic stimulation (TMS) studies (Dodds et al., 2010; Shao et al., 2016; Wittkuhn et al., 2017). Decision making involves the binary choice to either accept or reject an option based upon two competing attributes, i.e., the choice's anticipated costs and benefits. Previous studies have found that some participants prefer to reject offers for the rule of fairness to punish the proposer's unfair performance by conveying disgust and anger, and others could make an acceptance for reciprocity and benefits (Calder et al., 2001; Mujcic and Leibbrandt, 2017). The unfair condition, in particular, could induce conflict in the human between cognition ("accept") related to the dorsolateral prefrontal cortex and emotion ("reject") involving the anterior insula (Sanfey et al., 2003). The frontal cortex is widely known to be involved in human choice behavior, providing individuals with the ability to encode expected value representation and inhibition of proponent responses (Munakata et al., 2011). And the decision-making activations beginning in the visual cortex located in the occipital cortex and spreading to the prefrontal regions has also been revealed by a study with magneto-encephalography

Table 2
Prediction performance for the two datasets through the ERP amplitudes (EA), network properties (NP) and DSNP features.

Condition	Amplifier-1 ($\bar{x} \pm s$)			Amplifier-2 ($\bar{x} \pm s$)		
	LDA_DSNP	LDA_EA	LDA_NP	LDA_DSNP	LDA_EA	LDA_NP
S1	**0.88 ± 0.11**	0.52 ± 0.10	0.74 ± 0.20	**0.97 ± 0.06**	0.55 ± 0.11	0.72 ± 0.21
S2	**0.84 ± 0.20**	0.41 ± 0.14	0.59 ± 0.20	**0.86 ± 0.18**	0.42 ± 0.09	0.65 ± 0.24
S3	**0.93 ± 0.09**	0.45 ± 0.10	0.53 ± 0.19	**0.92 ± 0.10**	0.47 ± 0.09	0.64 ± 0.26

S1 for the extremely unfair condition; S2 for the moderately unfair condition; S3 for the fair condition.

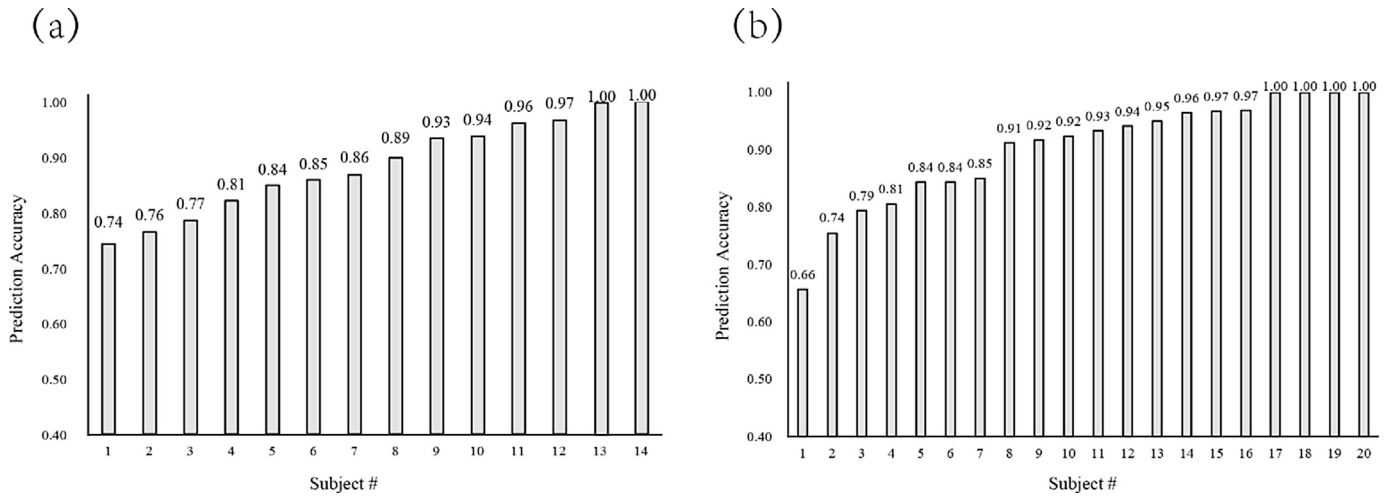

Fig. 6. The sorted prediction accuracies with DSNP for the two datasets. (a) amplifier-1; (b) amplifier-2.

(Pearson and Platt, 2012). Motivated from the spatial network topology difference revealed in both this and previous studies, we used the network topology information to perform the single-trial EEG based prediction.

However, different from the significant difference on spatial network patterns, the statistical network properties did not exhibit the obvious difference between the two responses in Fig. 4 (c). Specifically investigating the network topology in Fig. 4(b), both stronger (increased) and weaker (decreased) linkages could be found between the two responses, which accordingly alleviated the significant differences of the network properties between the two conditions and thereby might account for the insignificant difference in Fig. 4 (c). In essence, the challenge for the online prediction in current work is largely dependent on the signal quality of single trial EEG and the ERP component. Considering that the background noise in EEG is characterized with the relatively high frequency band, and the ERP components are reflected in the relatively low frequency band, to guarantee that a relatively stable MFN related EEG can be provided for the subsequent network analysis, we firstly used the 1–20 Hz band-pass filter as proposed in previous decision making studies to filter the EEG signals, which has been proved to be able to refine the MFN related information well (Hewig et al., 2011; Martin and Potts, 2011). Although the obvious spatial topology differences between the two responses could be observed, when the single-trial EEG is used to predict the response, the signal-to-noise rate is rather low, and it is difficult to extract the reliable spatial network patterns for single-trial prediction. Therefore, based on the constructed single-trial network, we specifically developed a supervised learning method (i.e., DSNP) to enhance the spatial difference of the single-trial network topology. The scalp topographies of the two DSNP filters in Fig. 4(a) demonstrated the working mechanism of DSNP. Specifically, combining the scalp topographies in Fig. 4(a) with the spatial difference of network topology in Fig. 4(b), the spatial filters estimated by DSNP imposed the large weights on the nodes experiencing denser linkage differences between the two responses while giving smaller weights to those nodes with fewer of linkages, which thus enhanced the importance of these nodes, i.e., enlarging the spatial topology difference of these nodes.

The scatter plots of DSNP features corresponding to the two DSNP filters in Fig. 5 further demonstrate that the proposed DSNP can extract the reliable features for both training and the online prediction. First, the training features represented by the asterisk are distributed with a clear LDA boundary. Second, the testing features derived from the learned DSNP filters show a similar distribution to the training features, i.e., most of the testing samples marked with circles are correctly distributed in the areas separated by the LDA boundary. This good separation characteristic of DSNP features revealed in Fig. 5 resulted in the better prediction performance in Table 1. When compared to the relatively lower performance of ERP amplitudes (i.e., 0.46 and 0.48) and network properties (i.e., 0.62 and 0.65), LDA based on the DSNP features achieved prediction accuracies of 0.88 and 0.90 for the two datasets. Although the MFN amplitude is an important index in decision-making processing, the MFN amplitudes could not always promise the satisfying classification performance in identifying distinct responses of decision. We assumed that this might be attributed to the huge variability of ERP across trials for each individual, and moreover the mere MFN amplitude could not reflect the information exchange among various brain areas, which had been proven to be important to fulfill the information processing during decision-making. Therefore, MFN amplitude based prediction achieves lower prediction performance compared to the two network based predictions. The difference between the network properties and DSNP features was consistent with that in Fig. 4, i.e., the significant difference of spatial network topology exhibited between the two responses while the insignificant difference for the network properties. In essence, while the subject will inevitably encounter the different conditions in the actual decision-making, he or she might have different responses. The prediction performances of the three fairness conditions (i.e., extremely unfair, moderately unfair and fair) further demonstrated that the proposed DSNP can reliably predict the individual responses in all three conditions with an accuracy above 0.84 for both datasets. As for the online decision prediction, a challenging problem is the large variability across subjects, which may hamper the practical application of the prediction system. Just as revealed in Fig. 6, the prediction accuracy largely varied across subjects (i.e., 0.74–1.00 for amplifier-1; 0.66–1.00 for amplifier-2), which has also been observed in other online prediction systems, such as brain-computer interface (Li et al., 2010; Long et al., 2012b; Zhang et al., 2015, 2016) and emotion recognition (Li et al., 2019b; Ricciardi et al., 2017; Yang et al., 2017). Although the huge variability existed, 28 out of the 34 subjects acquired single-trial prediction accuracies above 0.80. Even in those subjects with poor performance, the lowest accuracy was 0.66, which was much higher than the random accuracy of 0.50. These performances consistently demonstrated the proposed DSNP can availably extract the discriminative spatial network information to predict the decision responses for most subjects and then achieves a satisfying online prediction performance based on the single-trial EEG. Moreover, relative to previous studies, the EEG-based computational intelligence framework could effectively capture the variability of a single trial and also reflect the varied individual states.

Another advantage is the generalized ability of the DSNP to be used various datasets from different EEG systems in the actual application. In this study, we utilized two datasets recorded from different amplifiers to predict the responses between acceptance and rejection based upon the

single-trial EEG. The similar accuracies (0.88 for amplifier-1 and 0.90 for amplifier-2) between the two datasets can verify each other and provide credible evidence for the generalized merit of the proposed approach.

In this study, to simulate the online single-trial prediction, we divided the recording EEGs into the training and online prediction sets, where the former $N/2$ trials serve as the training set, and the remaining $N/2$ trials belong to the testing set. This strategy is close to the actual online prediction condition where subjects are required to perform the training before online prediction, then based on the trained model (i.e., LDA predictor and DSNP filters), the online single-trial prediction is made. When performing the online prediction, the time consumption needs to be considered. In the online prediction of current work, the network construction for the single trial EEG is determinative for the time consumption. As for the adopted coherence based network analysis, it has been proved to have the low computation complexity (Chorlian et al., 2009; Thatcher et al., 1986) and can satisfy the time requirement for the online prediction in current work.

5. Conclusion

Compared to previous studies focusing on the averaged measurements over multiple trials neglecting information about trial-to-trial variability, the current work captured this variability during the decision process and could also reflect the varied individual states of decision responses. In summary, based on the single-trial scalp UG-EEG, the proposed DSNP-based single-trial prediction method could reliably predict the instantaneous decision responses during decision-making, irrespective of the amplifiers used in the experiment. The prediction capacity was based on the inherent and implicit spatial information in brain EEG networks derived from single-trial EEG during decision-making. The DSNP helps us to discover the implicit information related to decision-making and therefore to create an intelligent decision system in the practical application as well.

Declaration of competing interest

None.

Acknowledgments

This work was supported by the National Natural Science Foundation of China (#61961160705, #81771925, #61603344, #61871423, and #71601136), the National Key Research and Development Plan of China (#2017YFB1002501), the Open Foundation of Henan Key Laboratory of Brain Science and Brain-Computer Interface Technology (No. HNBBL17001), the Longshan academic talent research supporting program of SWUST (#17LZX692). This work was funded in part by the Science and Technology Development Fund, Macau SAR (File no. 0045/2019/AFJ).

References

Bénar, C.G., Schön, D., Grimault, S., Nazarian, B., Burle, B., Roth, M., Badier, J.M., Marquis, P., Liegeois-Chauvel, C., Anton, J.L., 2007. Single-trial analysis of oddball event-related potentials in simultaneous EEG-fMRI. Hum. Brain Mapp. 28, 602–613.

Bartra, O., McGuire, J.T., Kable, J.W., 2013. The valuation system: a coordinate-based meta-analysis of BOLD fMRI experiments examining neural correlates of subjective value. Neuroimage 76, 412–427.

Basten, U., Biele, G., Heekeren, H.R., Fiebach, C.J., 2010. How the brain integrates costs and benefits during decision making. P. Natl. Acad. Sci. USA 107, 21767–21772.

Benjamin Blankertz, G.D., Krauledat, Matthias, Müller, Klaus-Robert, Gabriel, Curio, 2007. The non-invasive berlin brain-computer interface: fast acquisition of effective performance in untrained subjects. Neuroimage 37, 539–550.

Benjamin Blankertz, R.T., Lemm, Steven, Kawanabe, Motoaki, Müller, Klaus-Robert, 2008. Optimizing spatial filters for robust EEG single-trial analysis. IEEE Signal Process. Mag. 25.

Blankertz, B., Lemm, S., Treder, M., Haufe, S., Müller, K.-R., 2011. Single-trial analysis and classification of ERP components—a tutorial. Neuroimage 56, 814–825.

Boulgouris, N.V., Chi, Z.X., 2007. Gait recognition using radon transform and linear discriminant analysis. IEEE Trans. Image Process. 16, 731–740.

Buschman, T.J., Miller, E.K., 2007. Top-down versus bottom-up control of attention in the prefrontal and posterior parietal cortices. Science 315, 1860–1862.

Cai, T.T., Silverman, B.W., 2001. Incorporating information on neighbouring coefficients into wavelet estimation. Sankhya: Indian J. Stat. Ser. B 63, 127–148, 1960-2002.

Calder, A.J., Lawrence, A.D., Young, A.W., 2001. Neuropsychology of fear and loathing. Nat. Rev. Neurosci. 2, 352–363.

Cao, Z., Lin, C.T., Chen, M.H., Li, C.T., Su, T.P., 2018. Identifying ketamine responses in treatment-resistant depression using a wearable forehead EEG. IEEE T. Bio-Med. Eng. 66, 1668–1679.

Cecchetto, C., Korb, S., Rumiati, R.I., Aiello, M., 2017. Emotional Reactions in Moral Decision-Making Are Influenced by Empathy and Alexithymia. Soc Neurosci, UK, pp. 1–15.

Charpentier, C.J., De Neve, J., Li, X., Roiser, J.P., Sharot, T., 2016. Models of affective decision making: how do feelings predict choice? Psychol. Sci. 27, 763–775.

Chorlian, D.B., Rangaswamy, M., Porjesz, B., 2009. EEG coherence: topography and frequency structure. Exp. Brain Res. 198, 59.

Critchley, H.D., Elliott, R., Mathias, C.J., Dolan, R.J., 2000. Neural activity relating to generation and representation of galvanic skin conductance responses: a functional magnetic resonance imaging study. J. Neurosci. 20, 3033–3040.

Dixon, M.L., Andrews-Hanna, J.R., Spreng, R.N., Irving, Z.C., Mills, C., Girn, M., Christoff, K., 2017. Interactions between the default network and dorsal attention network vary across default subsystems, time, and cognitive states. Neuroimage 147, 632–649.

Dodds, C.M., Morein-Zamir, S., Robbins, T.W., 2010. Dissociating inhibition, attention, and response control in the frontoparietal network using functional magnetic resonance imaging. Cerebr. Cortex 21, 1155–1165.

Goudriaan, A.E., Oosterlaan, J.,., De, Beurs, E., Van Den, Brink, W., 2008. The role of self-reported impulsivity and reward sensitivity versus neurocognitive measures of disinhibition and decision-making in the prediction of relapse in pathological gamblers. Psychol. Med. 38, 41–50.

Hastie, R., 2001. Problems for judgment and decision making. Annu. Rev. Psychol. 52, 653–683.

Hewig, J., Kretschmer, N., Trippe, R.H., Hecht, H., Coles, M.G., Holroyd, C.B., Miltner, W.H., 2011. Why humans deviate from rational choice. Psychophysiology 48, 507–514.

Horat, S.K., Prévot, A., Richiardi, J., Herrmann, F.R., Favre, G., Merlo, M.C., Missonnier, P., 2017. Differences in social decision-making between proposers and responders during the Ultimatum Game: an EEG study. Front. Integr. Neurosci. 11, 13.

Hsu, W.Y., 2013. Embedded prediction in feature extraction: application to single-trial EEG discrimination. Clin. EEG Neurosci. 44, 31–38.

Hsu, W.Y., Lin, C.C., Ju, M.S., Sun, Y.N., 2007. Wavelet-based fractal features with active segment selection: application to single-trial EEG data. J. Neurosci. Methods 163, 145–160.

Koenigs, M., Tranel, D., 2007. Irrational economic decision-making after ventromedial prefrontal damage: evidence from the Ultimatum Game. J. Neurosci. 27, 951–956.

Krain, A.L., Wilson, A.M., Arbuckle, R., Castellanos, F.X., Milham, M.P., 2006. Distinct neural mechanisms of risk and ambiguity: a meta-analysis of decision-making. Neuroimage 32, 477–484.

Li, F., Chen, B., Li, H., Zhang, T., Wang, F., Jiang, Y., Li, P., Ma, T., Zhang, R., Tia, Y., 2016. The time-varying networks in P300: a task-evoked EEG study. IEEE T. Neur. Sys. Reh. 24, 725–733.

Li, F., Wang, J.J., Liao, Y., Yi, C., Jiang, Y., Si, Y., Peng, W., Yao, D., Zhang, Y., Dong, W., 2019a. Differentiation of schizophrenia by combining the spatial EEG brain network patterns of rest and task P300. IEEE T. Neur. Sys. Reh. 27, 594–602.

Li, F., Yi, C., Jiang, L.S.Y., Peng, W., Si, Y., Zhang, T., Zhang, R., Yao, D., Xu, Y.Z.P., 2018. Brain network reconfiguration during motor imagery revealed by a large-scale network analysis of scalp EEG. Brain Topogr. 32, 304–314.

Li, N., Ma, N., Liu, Y., He, X.-S., Sun, D.-L., Fu, X.-M., Zhang, X., Han, S., Zhang, D.-R., 2013. Resting-state functional connectivity predicts impulsivity in economic decision-making. J. Neurosci. 33, 4886–4895.

Li, P., Liu, H., Si, Y., Li, C., Li, F., Zhu, X., Huang, X., Zeng, Y., Yao, D., Zhang, Y., Peng, X., 2019b. EEG based emotion recognition by combining functional connectivity network and local activations. IEEE T. Bio-Med. Eng. 66, 1558–2531.

Li, Y., Jinyi, L., Yu, T., Yu, Z., Wang, C., Zhang, H., Guan, C., 2010. An EEG-based BCI system for 2-D cursor control by combining Mu/Beta rhythm and P300 potential. IEEE T. Bio-Med. Eng. 57, 2495–2505.

Long, J., Li, Y., Wang, H., Yu, T., Pan, J., Li, F., 2012a. A hybrid brain computer interface to control the direction and speed of a simulated or real wheelchair. IEEE T. Neur. Sys. Reh. 20, 720–729.

Long, J., Li, Y., Yu, T., Zhenghui, G., 2012b. Target selection with hybrid feature for BCI-based 2-D cursor control. IEEE T. Bio-Med. Eng. 59, 132.

LvC, W.Q., Chen, C., Qiu, J., Xue, G., He, Q., 2019. The regional homogeneity patterns of the dorsal medial prefrontal cortex predict individual differences in decision impulsivity. Neuroimage 200, 556–561.

Martin, L.E., Potts, G.F., 2011. Medial frontal event-related potentials and reward prediction: do responses matter? Brain Cogn. 77, 128–134.

Mika, S., Ratsch, G., Weston, J., Scholkopf, B., Mullers, K.R., 2002. Fisher Discriminant Analysis with Kernels. Neural Networks for Signal Processing Ix. IEEE Signal Processing Society Workshop.

Mueller, S.M., Schiebener, J., Delazer, M., Brand, M., 2018. Risk approximation in decision making: approximative numeric abilities predict advantageous decisions under objective risk. Cogn. Process. 1–19.

Mujcic, R., Leibbrandt, A., 2017. Indirect reciprocity and prosocial behaviour: evidence from a natural field experiment. Econ. J. 128, 1683–1699.

Munakata, Y., Herd, S.A., Chatham, C.H., Depue, B.E., Banich, M.T., O'Reilly, R.C., 2011. A unified framework for inhibitory control. Trends Cogn. Sci. 15, 453–459.
Neubert, F.-X., Mars, R.B., Sallet, J., Rushworth, M.F., 2015. Connectivity reveals relationship of brain areas for reward-guided learning and decision making in human and monkey frontal cortex. P. Natl. Acad. Sci. USA 112, E2695–E2704.
NK Glober, C.T., TM Abramson, K.S., 2019. A simple decision rule predicts futile resuscitation of out-of-hospital cardiac arrest. Resuscitation 142, 8–13.
Pearson, J., Platt, M.L., 2012. Dynamic decision making in the brain. Nat. Neurosci. 15, 341–342.
Peng Xu, P.Y., Xu, Lei, Yao, Dezhong, 2011. An enhanced probabilistic LDA for multi-class brain computer interface. PLoS One 6.
Peterburs, J., Voegler, R., Liepelt, R., Schulze, A., Wilhelm, S., Ocklenburg, S., Straube, T., 2017. Processing of fair and unfair offers in the ultimatum game under social observation. Sci. Rep-UK 7, 44062.
Preuss, N., Brändle, L.S., Hager, O.M., Haynes, M., Fischbacher, U., Hasler, G., 2016. Inconsistency and social decision making in patients with Borderline Personality Disorder. Psychiatry Res. 243, 115–122.
Ratcliff, R., Philiastides, M.G., Sajda, P., 2009. Quality of evidence for perceptual decision making is indexed by trial-to-trial variability of the EEG. Proc. Natl. Acad. Sci. U. S. A. 106, 6539–6544.
Ricciardi, L., Viscocomandini, F., Erro, R., Morgante, F., Bologna, M., Fasano, A., Ricciardi, D., Edwards, M.J., Kilner, J., 2017. Facial emotion recognition and expression in Parkinson's disease: an emotional mirror mechanism? PLoS One 12, e0169110.
S Debener, M.U., Siegel, M., Engel, A.K., 2006. Single-trial EEG–fMRI reveals the dynamics of cognitive function. Trends Cogn. Sci. 10, 558–563.
Sanfey, A.G., 2007. Social decision-making: insights from game theory and neuroscience. Science 318, 598–602.
Sanfey, A.G., Rilling, J.K., Aronson, J.A., Nystrom, L.E., Cohen, J.D., 2003. The neural basis of economic decision-making in the ultimatum game. Science 300, 1755–1758.
Shao, R., Sun, D., Lee, T., 2016. The interaction of perceived control and Gambler's fallacy in risky decision making: an fMRI study. Hum. Brain Mapp. 37, 1218.
Si, Y., Wu, X., Li, F., Zhang, L., Duan, K., Li, P., Song, L., Jiang, Y., Zhang, T., Zhang, Y., Chen, J., Gao, S., Biswal, B., Yao, D., Xu, P., 2018. Different decision-making responses occupy different brain networks for information processing: a study based on EEG and TMS. Cerebr. Cortex 29, 4119–4129.
Suzuki, S., Harasawa, N., Ueno, K., Gardner, J.L., Ichinohe, N., Haruno, M., Cheng, K., Nakahara, H., 2012. Learning to simulate others' decisions. Neuron 74, 1125–1137.
Thatcher, R.W., Krause, P.J., Hrybyk, M., 1986. Cortico-cortical associations and EEG coherence: a two-compartmental model ☆. Electroencephalogr. Clin. Neurophysiol. 64, 123–143.
Thatcher, R.W., North, D., Biver, C., 2005. EEG and intelligence: relations between EEG coherence, EEG phase delay and power. Clin. Neurophysiol. 116, 2129–2141.
Wang, G., Li, J., Li, Z., Wei, M., Li, S., 2016. Medial frontal negativity reflects advantageous inequality aversion of proposers in the ultimatum game: an ERP study. Brain Res. 1639, 38–46.
Wittkuhn, L., Eppinger, B., Bartsch, L.M., Thurm, F., Korb, F.M., Li, S.C., 2017. Repetitive transcranial magnetic stimulation over dorsolateral prefrontal cortex modulates value-based learning during sequential decision-making. Neuroimage 167, 384.
Wu, Y., Zhou, Y., E, v.D., 2011. Social comparison affects brain responses to fairness in asset division: an ERP study with the ultimatum game. Front. Hum. Neurosci. 5, 131.
Xu, P., Xiong, X., Xue, Q., Li, P., Zhang, R., Wang, Z., Valdes-Sosa, P.A., Wang, Y., Yao, D., 2014. Differentiating between psychogenic nonepileptic seizures and epilepsy based on common spatial pattern of weighted EEG resting networks. IEEE T. Bio-Med. Eng. 61, 1747–1755.
Yang, Y., Wu, Q.M.J., Zheng, W.L., Lu, B.L., 2017. EEG-based emotion recognition using hierarchical network with subnetwork nodes. IEEE Transac. Cogn. Dev. Sys. 10, 408–419.
Ye J, J.R., Li, Q., 2005. Two-dimensional linear discriminant analysis. Adv. Neural Inf. Process. Syst. 1569–1576.
Young, C.B., Raz, G., Everaerd, D., Beckmann, C.F., Tendolkar, I., Hendler, T., Fernández, G., Hermans, E.J., 2017. Dynamic shifts in large-scale brain network balance as a function of arousal. J. Neurosci. 37, 281–290.
Zhang, R., Yao, D., Valdés-Sosa, P.A., Li, F., Li, P., Zhang, T., Ma, T., Li, Y., Xu, P., 2015. Efficient resting-state EEG network facilitates motor imagery performance. J. Neural Eng. 12, 066024.
Zhang, T., Liu, T., Li, F., Li, M., Liu, D., Zhang, R., He, H., Li, P., Gong, J., Luo, C., 2016. Structural and functional correlates of motor imagery BCI performance: insights from the patterns of fronto-parietal attention network. Neuroimage 134, 475–485.